Original paper

Thermal behavior of uranyl selenite minerals derriksite and demesmaekerite

Vladislav V. GURZHIY[1]*, Alina R. IZATULINA[1], Maria G. KRZHIZHANOVSKAYA[1], Mikhail N. Murashko[1], Dar'ya V. SPIRIDONOVA[2], Vladimir V. SHILOVSKIKH[3], Sergey V. KRIVOVICHEV[1, 4]

[1] *Institute of Earth Sciences, St. Petersburg State University, University Emb. 7/9, St. Petersburg, 199034, Russian Federation; vladislav.gurzhiy@spbu.ru, vladgeo17@mail.ru*

[2] *Research Centre for X-ray Diffraction Studies, St. Petersburg State University, Universitetskiy ave. 26, St. Petersburg, 198504, Russian Federation*

[3] *Centre for Geo-Environmental Research and Modelling ("Geomodel"), St. Petersburg State University, Ulyanovskaya str. 1, St. Petersburg, 198504, Russian Federation*

[4] *Nanomaterials Research Centre, Kola Science Centre, Russian Academy of Sciences, Fersmana 14, 184209, Apatity, Russian Federation*

[*] *Corresponding author*

Crystal structures of two uranyl selenite minerals derriksite, $Cu_4[(UO_2)(SeO_3)_2](OH)_6$, and demesmaekerite, $Pb_2Cu_5[(UO_2)_2(SeO_3)_6(OH)_6](H_2O)_2$, which structures are based on uranyl selenite 1D structural units, were studied employing single-crystal X-ray diffraction analysis at various temperatures. The refinement of their crystal structures reveals the detailed dynamics of the interatomic interactions during the heating process, which allows describing the thermal behavior. Uranyl selenite chains and their mutual arrangement mainly provide the rigidity of the crystal structure. Thus the lowest expansion in the structure of derriksite is observed along the direction of uranyl selenite chains, while the largest expansion occurs in the direction normal to chains, with the space occupied by lone electron pairs of Se^{4+} atoms and low covalent bond distribution density. The maximal expansion in the crystal structure of demesmaekerite is manifested approximately along the [100], which matches the direction of chains of less strongly bonded Cu-centered octahedra, and gaps between Cu chains occupied by the Pb cations. The crystal structure of demesmaekerite undergoes contraction in the direction of the space between the U-bearing chains with the deficiency of strong covalent bonds. Contraction of the structure can also be attributed to the orthogonalization of the oblique triclinic angles of the unit cell. It is demonstrated that the assignment of U-bearing units during structure description is reasonably justified since, regardless of their dimensionality, these substructural units are one of the most stable and rigid blocks in the structural architecture, and they govern the thermal behavior of the entire structure.

Keywords: derriksite, demesmaekerite, uranyl, selenite, crystal structure, thermal expansion
Received: 23 September 2020; accepted: 30 November 2020; handling editor: J. Plášil
Electronic supplementary material. Supplementary crystallographic data for this paper are available online at the Journal web site (http://dx.doi.org/10.3190/jgeosci.315).

1. Introduction

Uranyl selenite minerals represent a rather rare group of secondary U^{6+}-bearing natural phases that were described only in a few localities in the world. Those are, primarily, Musonoi and Shinkolobwe in DR Congo, Repete mine in Utah (USA), Zálesí deposit in the Czech Republic, Liauzun in France, and La Creusaz U prospect in Switzerland, and Eureka mine in Spain (Lussier et al. 2016; Gurzhiy et al. 2019a). There are seven uranyl selenite minerals known up to date: guilleminite, $Ba[(UO_2)_3(SeO_3)_2O_2](H_2O)_3$ (Pierrot et al. 1965), demesmaekerite, $Pb_2Cu_5[(UO_2)_2(SeO_3)_6(OH)_6](H_2O)_2$ (Cesbron et al. 1965), marthozite, $Cu[(UO_2)_3(SeO_3)_2O_2](H_2O)_8$ (Cesbron et al. 1969), derriksite, $Cu_4[(UO_2)(SeO_3)_2](OH)_6$ (Cesbron et al. 1971), haynesite, $[(UO_2)_3(SeO_3)_2(OH)_2](H_2O)_5$ (Deliens and Piret 1991), piretite, $Ca(UO_2)_3(SeO_3)_2(OH)_4 \cdot 4H_2O$ (Vochten et al. 1996), and larisaite, $Na(H_3O)[(UO_2)_3(SeO_3)_2O_2](H_2O)_4$ (Chukanov et al. 2004), and their characterization is far from being complete. Thus, the crystal structures of only five minerals from this group have been reported to date, while those for piretite and haynesite are still not determined, but the vibrational spectroscopy data were obtained and studied for all seven species (Vochten et al. 1996; Chukanov et al. 2004; Frost et al. 2006, 2008a,b, 2009a,b, 2014). Thermal stability of guilleminite (Pierrot et al. 1965), marthozite (Cesbron et al. 1969), derriksite

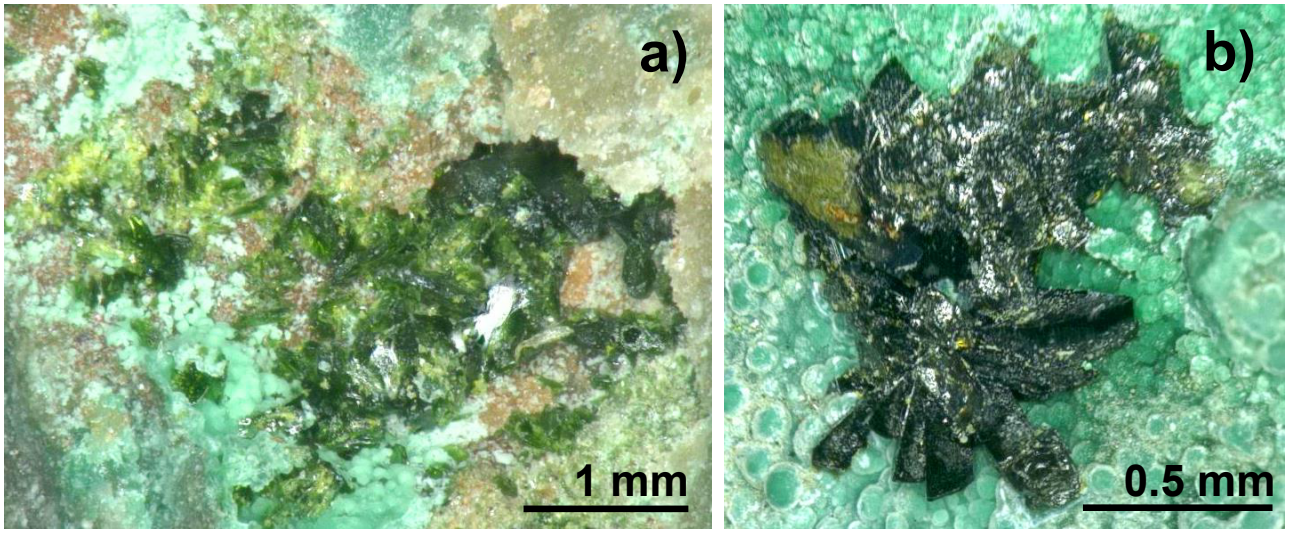

Fig. 1 Crystalline aggregates of olive-green derriksite (a) and brownish-green demesmaekerite (b) in association with light-green malachite.

(Cesbron et al. 1971) and piretite (Vochten et al. 1996) were studied using the TGA technique in the temperature range of 25–1000 °C.

With the current work, we fill in a number of crystal-chemical gaps related to the named group of compounds. Single crystals of derriksite and demesmaekerite were studied using a single-crystal X-ray diffraction technique in the temperature range of –173 to +87 °C, which allow revealing the thermal behavior of their crystal structures.

2. Materials and methods

2.1. Samples and occurrence

The single crystals of secondary uranyl selenite minerals derriksite (**DER**) and demesmaekerite (**DEM**) studied in this work (Fig. 1) were taken from the private collection of the author of the current paper (from V.V.G., sample 6111). The sample originates from the Musonoi, DR Congo.

2.2. Chemical composition

Small pieces of the **DER** and **DEM** single crystals verified on the diffractometer were crushed, pelletized and carbon-coated. The elemental composition of the samples was determined using a Hitachi S-3400N scanning electron microscope equipped with a AzTec Energy X-Max 20 spectrometer, with an acquisition time of 60 s per point (acceleration voltage 20 kV, beam current 2 nA) and processed with Oxford AzTec software with TrueQ technique. The following analytical standards were used: chalcopyrite (CuK_α), Se (SeL_α), uranium containing glass (UM_α), PbTe (PbM_α). Analytical calculations for **DER**: atomic ratio from structural data Cu 4.00, U 1.00, Se 2.00; found by EDX: Cu 3.95, U 1.04, Se 2.01. Analytical calculations for **DEM**: atomic ratio from structural data Pb 2.00, Cu 5.00, U 2.00, Se 6.00; found by EDX: Pb 2.09, Cu 4.90, U 2.06, Se 5.95. Traces of Si up to 0.5 at. % were found by EDX that can be attributed to the micro inclusions of quartz.

2.3. Single-crystal X-ray diffraction study

Single crystals of **DER** and **DEM** were selected under an optical microscope, encased in epoxy resin, and mounted on cryoloops. Diffraction data were collected using a Rigaku Oxford Diffraction SuperNova diffractometer equipped with an Atlas CCD detector operated with monochromated microfocused MoKα radiation (λ = 0.71073 Å) at 50 kV and 0.8 mA. Diffraction data were collected at different temperatures without changing the crystal orientation in the range of –173 to +87 °C (Tab. 1) with frame widths of 1.0° in ω, and exposures of 22.5 s per frame. Data were integrated and corrected for background, Lorentz, and polarization effects. An analytical (numeric) absorption correction using a multifaceted crystal model based on expressions derived by Clark and Reid (1995) was applied in the *CrysAlisPro* (2018) program. The unit-cell parameters (Tab. 1) were refined using least-squares techniques. The structures were solved by a dual-space algorithm and refined using the *SHELX* programs (Sheldrick 2015a, b) incorporated in the *OLEX2* program package (Dolomanov et al. 2009). The final models included coordinates and anisotropic displacement parameters for all non-H atoms. The H atoms of OH^- groups and H_2O molecules were localized from difference Fourier maps and were included in the refinement with U_{iso}(H) set to 1.5U_{eq}(O) and O–H restrained to 0.95 Å. Selected interatomic distances and angles are listed in the Tabs 2 and 3. Supplementary crystallographic data obtained in the

Tab. 1 Crystallographic data and refinement parameters for derriksite (**DER**) and demesmaekerite (**DEM**) single crystals

Crystal	S.G.	*T* [°C]	*a* [Å] / *α* [°]	*b* [Å] / *β* [°]	*c* [Å] / *γ* [°]	*V* [Å^3]	R_1 ($\|Fo\| \geq 4\sigma F$)	*ICSD entry*
DER	$Pmn2_1$	–173	5.9679(3)	5.5501(3)	19.0613(9)	631.35(5)	0.0391	2033196
		–120	5.9689(3)	5.5534(4)	19.0643(10)	631.93(6)	0.0358	2033197
		–80	5.9693(2)	5.5579(3)	19.0674(7)	632.59(5)	0.0341	2033198
		–40	5.9702(2)	5.5629(3)	19.0733(8)	633.46(5)	0.0368	2033199
		0	5.9720(3)	5.5688(4)	19.0840(11)	634.67(7)	0.0364	2033200
		30	5.9743(4)	5.5759(4)	19.0983(11)	636.20(7)	0.0433	2033201
		60	5.9784(3)	5.5874(4)	19.1254(11)	638.86(7)	0.0448	2033202
		87	5.9843(3)	5.5966(4)	19.1599(10)	641.69(6)	0.0472	2033203
DEM	*P*–1	–173	5.6320(4) / 88.622(3)	10.0417(3) / 79.572(4)	11.9844(4) / 89.699(4)	666.39(6)	0.0337	2033206
		–130	5.6406(3) / 88.638(4)	10.0492(4) / 79.578(5)	11.9810(8) / 89.763(4)	667.73(7)	0.0343	2033207
		–90	5.6456(3) / 88.654(4)	10.0564(4) / 79.604(4)	11.9803(6) / 89.804(4)	668.82(5)	0.0327	2033208
		–60	5.6548(3) / 88.649(4)	10.0640(5) / 79.611(5)	11.9794(7) / 89.824(4)	670.38(7)	0.0321	2033209
		–30	5.6594(5) / 88.659(3)	10.0663(4) / 79.634(5)	11.9792(5) / 89.844(5)	671.12(7)	0.0348	2033210
		0	5.6611(4) / 88.658(3)	10.0691(3) / 79.631(4)	11.9759(4) / 89.878(4)	671.31(5)	0.0354	2033211
		30	5.6628(3) / 88.670(4)	10.0773(4) / 79.684(4)	11.9753(6) / 89.912(4)	672.16(5)	0.0342	2033212
		60	5.6660(3) / 88.671(3)	10.0840(4) / 79.718(4)	11.9746(5) / 89.932(3)	673.00(5)	0.0345	2033213
		87	5.6699(5) / 88.674(4)	10.0953(4) / 79.773(6)	11.9744(7) / 89.940(5)	674.33(8)	0.0361	2033214

S.G. – space group symbol

range of –173 to +87 °C were deposited in the Inorganic Crystal Structure Database (ICSD) and can be obtained by quoting the depository numbers CSD 2033196–2033203 (**DER**) and 2033206–2033214 (**DEM**) *via* www.ccdc.cam.ac.uk/structures/. It should be noted that the crystal structures of derriksite (Ginderow and Cesbron 1983b) and demesmaekerite (Ginderow and Cesbron 1983a; Gurzhiy et al. 2019a) have been reported previously, and our studies confirm those structural models, but the use of good quality crystals and modern XRD equipment made it possible to refine the structures of minerals with higher precision.

2.4. Thermal expansion tensor calculations

The main coefficients of the thermal-expansion tensor were determined using a second-order approximation of temperature dependencies for the unit cell parameters by means of the TEV software (Langreiter and Kahlenberg 2015). The TEV program was also used to determine the orientation of the principal axes of the thermal expansion tensor and for the visualization of the figure of thermal expansion/contraction coefficients (TEC).

3. Results and Discussion

3.1. Structure Descriptions

There is one symmetrically unique U atom in the structure of **DER**, forming an approximately linear UO_2^{2+}

Tab. 2 Selected geometrical parameters (bond lengths, Å; and angles, °) in the structure of **DER**

		–173 °C	87 °C			–173 °C	87 °C
U1–O1		1.802(18)	1.79(3)	Cu3–O6		2.438(15)	2.46(2)
U1–O2		1.776(18)	1.77(3)	Cu3–HO7	×2	1.973(12)	1.966(14)
<U1–O_{ur}>		1.789	1.78	Cu3–HO8		2.374(16)	2.39(2)
U1–O3	×2	2.271(12)	2.284(16)	Cu3–HO10	×2	1.970(10)	1.972(12)
U1–O5	×2	2.315(13)	2.324(17)	<Cu3–O>		2.116	2.12
<U1–O_{eq}>		2.293	2.30				
Se1–O3	×2	1.736(13)	1.726(19)	U1–O3–Se1		143.2(7)	143.5(12)
Se1–O4		1.666(15)	1.67(2)	U1–O5–Se2		143.3(8)	143.5(11)
<Se1–O>		1.713	1.71	Se1–O4–Cu1		135.7(4)	136.0(6)
Se2–O5	×2	1.720(12)	1.715(18)	Se1–O4–Cu2		122.6(8)	122.4(11)
Se2–O6		1.653(15)	1.64(2)	Se2–O6–Cu1		127.6(5)	127.8(8)
<Se2–O>		1.698	1.69	Se2–O6–Cu3		138.8(9)	138.8(12)
Cu1–O4		2.391(12)	2.402(16)	Cu1–O4–Cu1		77.3(5)	77.1(6)
Cu1–O6		2.398(13)	2.436(18)	Cu1–O4–Cu2		83.1(4)	82.8(6)
Cu1–HO7		1.982(13)	2.015(15)	Cu1–O6–Cu1		76.9(5)	75.7(6)
Cu1–HO8		1.912(10)	1.914(12)	Cu1–O6–Cu3		82.2(4)	81.5(6)
Cu1–HO9		1.922(10)	1.927(13)	Cu1–HO7–Cu2		103.6(5)	103.7(6)
Cu1–HO10		2.014(11)	2.044(14)	Cu3–HO7–Cu1		106.9(5)	106.9(7)
<Cu1–O>		2.103	2.12	Cu3–HO7–Cu2		97.2(5)	98.0(6)
Cu2–O4		2.399(16)	2.44(2)	Cu1–HO8–Cu1		102.4(7)	102.7(9)
Cu2–HO7	×2	2.008(11)	2.000(13)	Cu1–HO8–Cu3		93.0(5)	93.3(7)
Cu2–HO9		2.267(16)	2.283(19)	Cu1–HO9–Cu1		102.0(7)	102.0(9)
Cu2–HO10	×2	1.958(10)	1.969(12)	Cu1–HO9–Cu2		96.5(5)	96.7(6)
<Cu2–O>		2.100	2.11	Cu2–HO10–Cu1		106.2(5)	105.6(6)
				Cu2–HO10–Cu3		98.9(5)	98.8(6)
				Cu3–HO10–Cu1		103.4(5)	103.3(6)

Tab. 3 Selected geometrical parameters (bond lengths, Å; and angles, °) in the structure of **DEM**

		–173 °C	87 °C			–173 °C	87 °C
U1–O1		1.777(7)	1.772(8)	Cu3–O7		2.049(7)	2.060(8)
U1–O2		1.792(7)	1.780(8)	Cu3–O10		2.025(7)	2.041(8)
<U1–O_{Ur}>		1.785	1.776	Cu3–HO12		2.366(6)	1.950(7)
U1–O3		2.393(6)	2.394(6)	Cu3–HO12		1.956(6)	2.372(7)
U1–O5		2.465(6)	2.477(6)	Cu3–HO13		1.958(6)	1.944(7)
U1–O6		2.355(6)	2.361(7)	Cu3–H_2O15		2.386(7)	2.407(9)
U1–O8		2.349(7)	2.363(7)	<Cu3–O>		2.123	2.129
U1–O9		2.374(6)	2.377(6)				
<U1–O_{eq}>		2.387	2.394	U1–O3–Se1		119.6(4)	120.5(4)
Se1–O3		1.719(6)	1.710(7)	U1–O5–Se1		125.2(3)	125.7(3)
Se1–O4		1.699(6)	1.709(6)	U1–O6–Se2		139.1(4)	140.2(5)
Se1–O5		1.719(7)	1.716(7)	U1–O8–Se2		144.3(4)	143.5(5)
<Se1–O>		1.712	1.712	U1–O9–Se3		124.9(3)	126.5(4)
Se2–O6		1.710(6)	1.694(7)	Se1–O4–Pb1		125.0(3)	124.0(3)
Se2–O7		1.710(6)	1.703(6)	Se1–O4–Cu2		130.0(4)	130.3(4)
Se2–O8		1.691(7)	1.680(9)	Se1–O5–Pb1		121.6(3)	121.8(3)
<Se2–O>		1.704	1.692	Se2–O7–Cu1		129.8(4)	130.0(4)
Se3–O9		1.687(7)	1.673(8)	Se2–O7–Cu3		120.9(4)	122.1(5)
Se3–O10		1.708(6)	1.705(7)	Se3–O10–Cu1		138.3(3)	137.8(4)
Se3–O11		1.725(6)	1.712(6)	Se3–O10–Cu3		116.8(4)	116.6(4)
<Se3–O>		1.707	1.697	Se3–O11–Pb1		107.9(3)	108.4(3)
Pb1–O4		2.748(6)	2.754(7)	Se3–O11–Cu2		122.1(3)	123.0(3)
Pb1–O5		2.642(6)	2.644(7)	Se3–O11–Cu2		116.1(4)	116.0(4)
Pb1–O6		2.932(6)	2.924(7)	Cu2–O4–Pb1		99.1(2)	100.3(2)
Pb1–O7		3.068(7)	3.085(7)	Cu3–O7–Cu1		102.8(2)	102.2(2)
Pb1–O10		2.934(6)	2.949(7)	Cu3–O10–Cu1		95.2(2)	95.0(3)
Pb1–O11		2.536(6)	2.567(6)	Cu2–O11–Pb1		98.1(2)	97.4(2)
Pb1–HO13		2.376(6)	2.390(7)	Cu2–O11–Pb1		105.9(2)	105.4(2)
Pb1–HO14		2.484(6)	2.496(7)	Cu2–O11–Cu2		104.3(3)	103.9(3)
Pb1–H_2O15		3.099(8)	3.111(10)	Cu1–HO12–Cu3		100.5(2)	101.7(2)
<Pb1–O>		2.758	2.769	Cu1–HO12–Cu3		107.5(3)	107.6(3)
Cu1–O7	×2	2.193(7)	2.240(7)	Cu3–HO12–Cu3		93.5(3)	93.2(3)
Cu1–O10	×2	2.222(6)	2.208(7)	Cu2–HO13–Pb1		92.3(2)	92.1(2)
Cu1–HO12	×2	1.935(7)	1.933(7)	Cu3–HO13–Pb1		114.3(3)	115.1(3)
<Cu1–O>		2.117	2.127	Cu3–HO13–Cu2		130.3(4)	130.5(4)
Cu2–O4		1.984(6)	1.978(6)	Cu2–HO14–Pb1		112.1(3)	112.4(3)
Cu2–O11		2.380(6)	2.403(7)	Cu2–HO14–Pb1		101.8(2)	102.5(3)
Cu2–O11		2.003(6)	2.026(7)	Cu2–HO14–Cu2		98.3(3)	98.3(3)
Cu2–HO13		2.426(7)	2.452(7)				
Cu2–HO14		1.982(6)	1.956(7)				
Cu2–HO14		1.956(7)	1.989(6)				
<Cu2–O>		2.122	2.134				

uranyl ions (*Ur*) with two short $U^{6+}\equiv O^{2-}$ bonds (Tab. 2). In the equatorial plane, *Ur* cation is coordinated by four O_{eq} atoms that belong to selenite groups to form a tetragonal bipyramid as a coordination polyhedron of U atoms. There are two crystallographically nonequivalent Se atoms (Se as tetravalent) in the structure of **DER**, which are arranged in the apical vertex of a trigonal pyramid, surrounded by three O atoms. Selenite ions possess classical coordination geometry with the lone-electron pair squeezes O ligands toward the other side of the Se^{4+} cation, while the pair itself arranges and behaves like the fourth vertex of the regular tetrahedron. All four O_{eq} atoms are shared with the $[SeO_3]^{2-}$ groups, whereas each selenite group has only two O atoms shared with two neighbors *Ur*, which results in the formation of an infinite chain as the main structure building block (Fig. 2a). Chains pass along the [001] and the equatorial planes of *Ur* tetragonal bipyramids are arranged parallel to the (101). There are three crystallographically non-equivalent Cu atoms in the structure of **DER**, which possess distorted octahedral coordination with nearly square equatorial plane of OH^- groups and elongated apical contacts with O atoms due to the Jahn-Teller effect. Each Cu atom shares its equatorial hydroxyl groups with the neighbor Cu atoms, forming tri-octahedral layers (Fig. 2c) parallel to (010). Copper-oxygen layers are linked with uranyl selenite chains through the *trans*- arranged apical O atoms, which are the third vertices of selenite groups non-shared with *Ur* (Fig. 3). Additional linkage is made through the H-bonding system, which involves hydroxyl groups from the Cu–O layer and both O_{Ur} and O_{eq} from the U-bearing chains (OH7···O3, OH8···O1, OH9···O5, OH10···O5). Stereochemically active lone-electron pairs of the Se^{4+} cations are directed towards the neighbor uranyl selenite chains.

Uranyl selenite chain in the structure of **DER** corresponds to one of the simplest and common *cc*1–1:2–1 topological types (Fig. 2b). Its graph can be described as an infinite chain of 4-membered vertex-sharing rings (Krivovichev 2008). For instance, the same topology was observed in the structure of kröhnkite, $Na_2Cu(SO_4)_2(H_2O)_2$ (Hawthorne and Ferguson 1975), uranyl sulfate mineral rietveldite, $Fe(UO_2)(SO_4)_2(H_2O)_5$ (Kampf et al. 2017) and its Mg-bearing synthetic analogs $Mg[(UO_2)(TO_4)_2(H_2O)](H_2O)_4$ (T = S, Se) (Gurzhiy et al. 2019b).

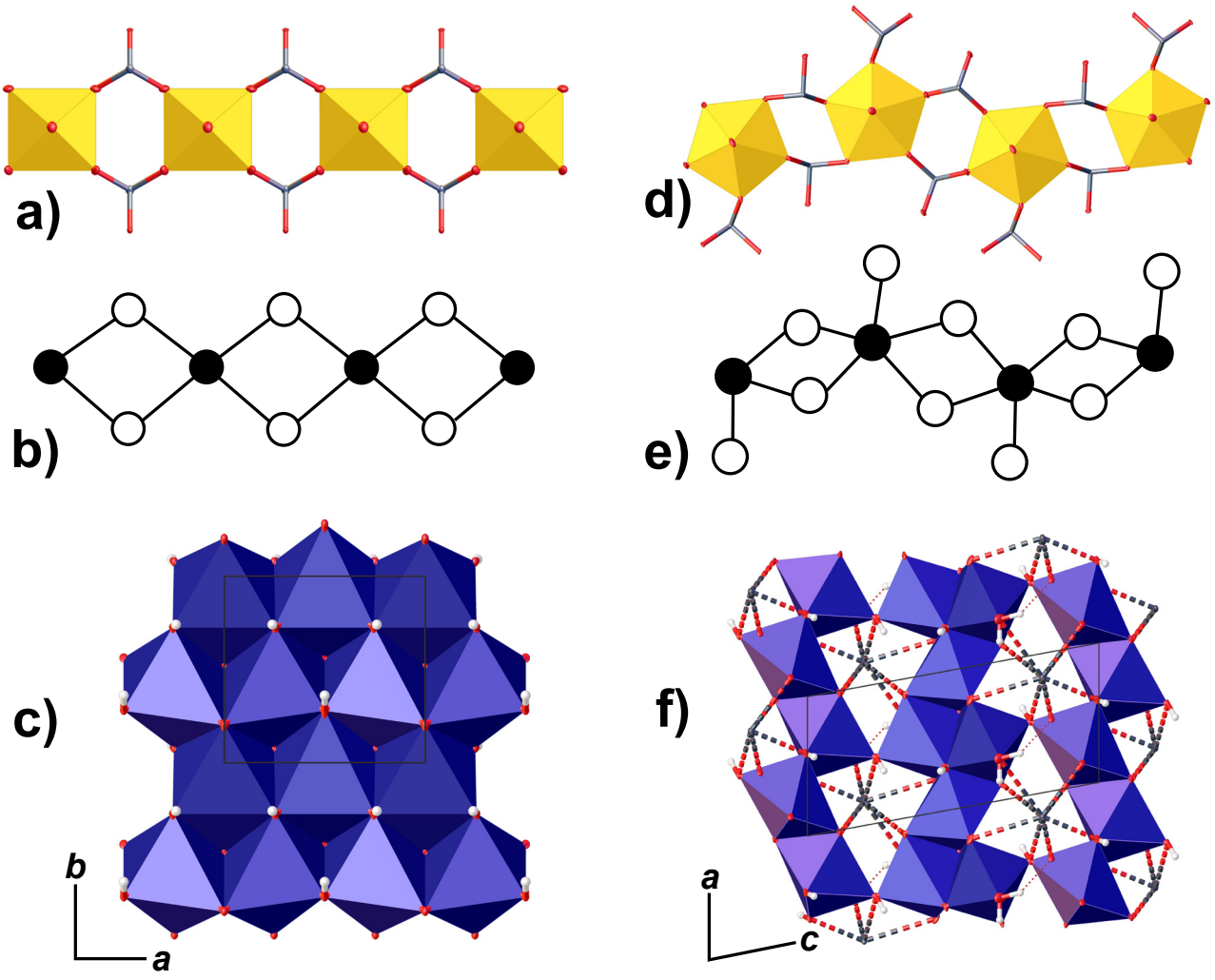

Fig. 2 a – Uranyl selenite chain in the structure of **DER. b** – its graphical representation. **c** – trioctahedral layer in the structure of **DER** built by Cu-centered $[CuO_2(OH)_4]$ complexes. **d** – uranyl selenite chain in the structure of **DEM**, and **e** – its graphical representation. **f** – interstitial layer built by Cu-centered octahedra and Pb-centered nine-fold polyhedra in the structure of **DEM**. Color scheme: U polyhedra = yellow; Cu polyhedra = dark blue; Se, Pb and O atoms are grey, dark grey and red, respectively; hydrogen atoms are small white circles; Pb–O bonds = dark grey stippled cones; black nodes = U atoms, white nodes = Se atoms.

There is one symmetrically unique U atom in the structure of **DEM**, forming *Ur* with two short $U^{6+}\equiv O^{2-}$ bonds and another five O_{eq} atoms that belong to selenite groups, to form a pentagonal bipyramid as a coordination polyhedron of U atoms (Tab. 3). There are three crystallographically non-equivalent Se atoms in the structure of **DER** arranged in the apical vertices of trigonal pyramids, surrounded by three O atoms. Se1- and Se2-centered groups have two O atoms shared with two neighboring *Ur*, while the third Se3-centered group has only one O atom shared with *Ur*, which results in the formation of infinite uranyl selenite 1D unit (Fig. 2d). The *Ur* shares four O_{eq} atoms with 2-connected selenite groups, and the fifth vertex is occupied by another 1-connected $[SeO_3]^{2-}$ pyramid. Uranyl selenite 1D units are arranged along the [101], having the equatorial planes of *Ur* pentagonal bipyramids being parallel to (101). Chains are stacked one above the other, forming blocks parallel to (010) (Fig. 4). These blocks, in turn, are separated by the sheets of edge-shared Cu- and Pb-centered coordination polyhedra (Fig. 2f). There are three crystallographically non-equivalent Cu atoms in the structure of **DEM**, which possess three different coordination geometries $[Cu1O_4(OH)_2]^{8-}$, $[Cu2O_3(OH)_3]^{7-}$ and $[Cu3O_2(OH)_3(H_2O)]^{6-}$, and one non-equivalent Pb^{2+} cation is arranged in the center of ninefold $[PbO_6(OH)_2(H_2O)]^{12-}$ complex. Cu1 atoms possess (2+4) distorted geometry, while Cu2 and Cu3 atoms have (4+2) coordination, which is considered to be more stable. Hathaway (1984) have shown that Cu^{2+}-bearing polyhedra with the (2+4) geometry may be the case of the dynamic Jahn-Teller effect of a series of (4+2) complexes that are rapidly interchanging at various temperatures. However, we did not find such an effect within current data. Cu-centered polyhedra form two types of chains directed along the

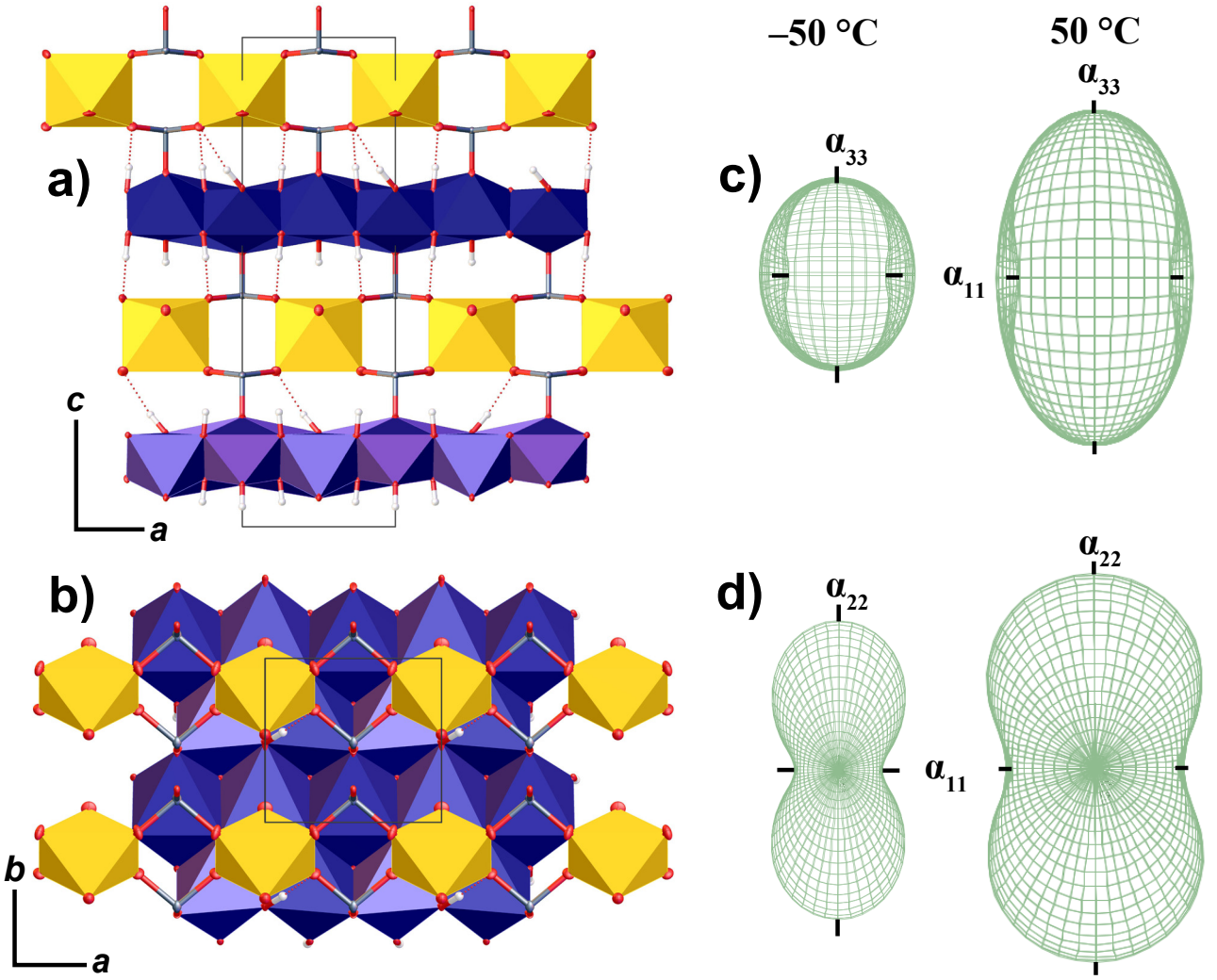

Fig. 3 The crystal structure of **DER. a** – projected along the *b* axis. **b** –projected along the *c* axis (b). **c, d** – the arrangement of figures of thermal expansion/contraction coefficients (TEC) relative to the structure projections. Color scheme same as in Fig. 2; TEC figures: expansion = green, contraction = red.

[100] and linked together *via* Pb-centered complexes and a common O13H group. The first type is formed by the alternating …–one Cu1–two Cu3–one Cu1–two Cu3–… octahedra with an edge-sharing linkage. There, the Cu1 octahedron shares four of its edges with four Cu3 polyhedra, and Cu3 shares two edges with two Cu1 octahedra, one edge with neighboring Cu3. This type of connection is a shortcutting of the trioctahedral layer in **DER**. The second type is a narrow, one octahedron wide chain built by Cu2-centered polyhedra that are connected only through the two common edges.

The topology of the U–Se chain in the structure of **DEM** belongs to the *cc*1–1:3–2 type (Krivovichev 2008) and has some similarities with that for **DER** (vertex-sharing infinite chain of 4-membered rings), but also has a very distinct difference in the additional 1-connected selenite group to each *Ur* (Fig. 2e), which makes this topology relatively rare. It has been observed in a few structures of exclusively synthetic U-bearing compounds, e.g. $(C_2H_8N)_3[(UO_2)(SeO_4)_2(HSeO_4)]$ (Gurzhiy et al. 2017).

It should be noted that derriksite and demesmaekerite are the only uranyl selenite minerals, which structures are built upon infinite 1D U-bearing units. Crystal structures of guilleminite, marthozite, haynesite, piretite, and larisaite are based on dense uranyl selenite layers of the phosphuranylite topology (Demartin et al. 1991; Gurzhiy et al. 2019a).

3.2. Thermal Behavior

There is a beahvior of the unit-cell parameters of **DER** versus temperature shown in Figure 5. All parameters are gradually increasing with temperature. However, *a* unit cell parameter grows very slowly and *b*, on the contrary, rises sharply. Equations describing the temperature dependence of the unit cell parameters of **DER** within the

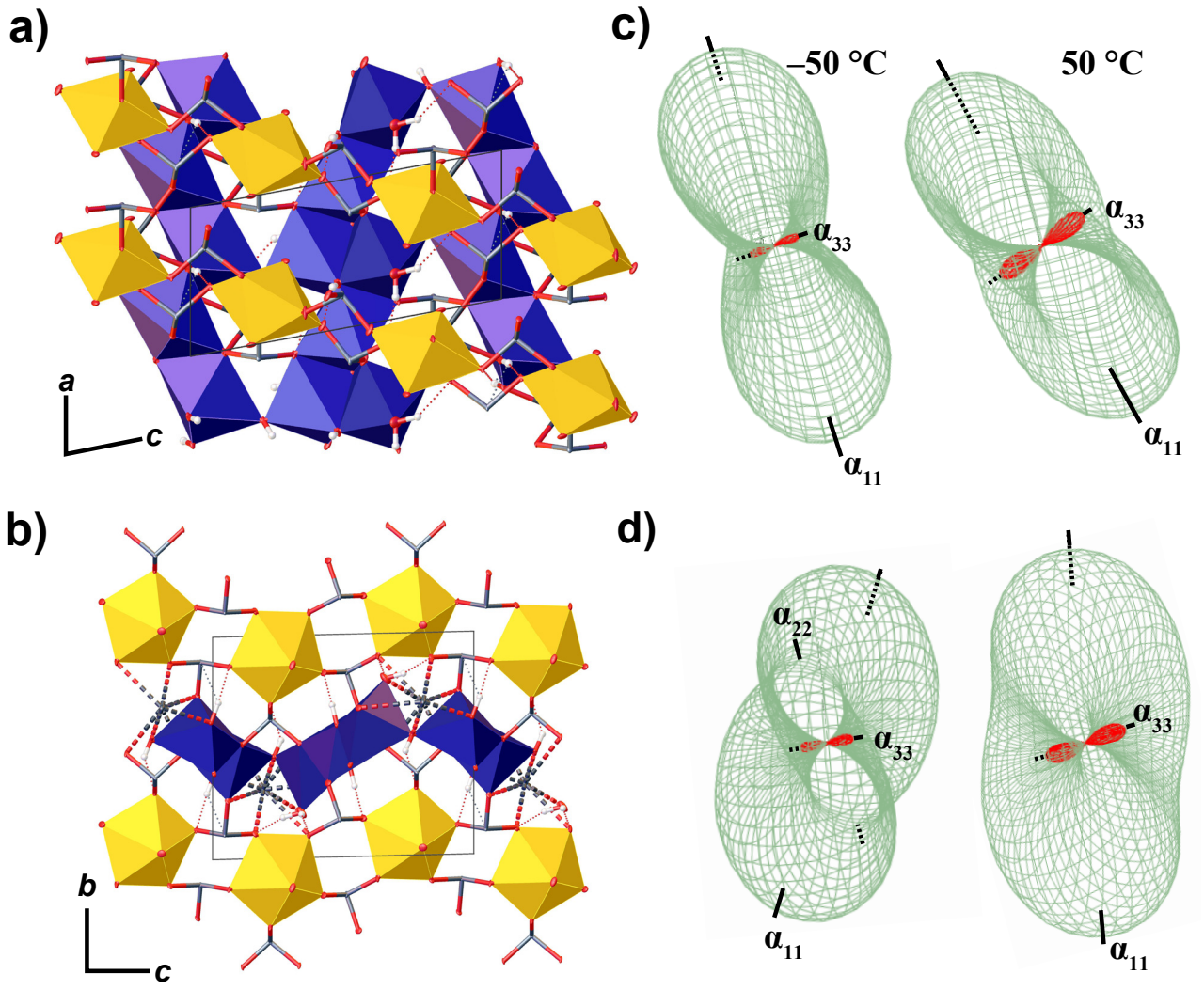

Fig. 4 The crystal structure of **DEM. a** – projected along the *b* axis. **b** – projected along the*a* axis (b). **c, d** – the arrangement of figures of thermal expansion/contraction coefficients (TEC) relative to the structure projections. Color scheme same as in Figs. 2 and 3.

range of –173 to 87 °C are: $a = 5.972 + 8.278 \times 10^{-5} \times T + 3.399 \times 10^{-7} \times T^2$; $b = 5.569 + 2.276 \times 10^{-4} \times T + 6.486 \times 10^{-7} \times T^2$; $c = 19.084 + 5.154 \times 10^{-4} \times T + 2.158 \times 10^{-6} \times T^2$; and $V = 634.7 + 52.8 \times 10^{-3} \times T + 1.9 \times 10^{-4} \times T^2$.

The Fig. 6 shows the behavior of the unit-cell parameters of **DEM** as a function of temperature. The dependence here is not so regular and more complicated than it was observed for **DER**. The largest increase is observed for the *a* unit-cell parameter, while the *c* decreases with temperature increase, although slightly. There are also different characters of functions are observed for various parameters. Thus, *b* and *β* are described by nearly exponential growth; *a*, *α* and *γ* functions flatten out with temperature increase, while the *c* is described by decreasing almost linear function. Equations describing the temperature dependence of the unit-cell parameters of **DEM** within the range of –173 to 87 °C are: $a = 5.661 + 1.139 \times 10^{-4} \times T - 3.204 \times 10^{-7} \times T^2$; $b = 10.069 + 2.140 \times 10^{-4} \times T + 2.689 \times 10^{-7} \times T^2$; $c = 11.976 - 3.657 \times 10^{-5} \times T + 4.328 \times 10^{-8} \times T^2$; $\alpha = 88.66 + 1.506 \times 10^{-4} \times T - 4.415 \times 10^{-7} \times T^2$; $\beta = 79.63 + 9.491 \times 10^{-4} \times T + 2.983 \times 10^{-6} \times T^2$; $\gamma = 89.88 + 8.353 \times 10^{-4} \times T - 1.120 \times 10^{-6} \times T^2$; and $V = 671.3 + 27.9 \times 10^{-3} \times T - 1.3 \times 10^{-5} \times T^2$.

The thermal behavior of **DER** and **DEM** has a substantially anisotropic character (Tab. 4). The general theory of thermal behavior (Filatov 1990, 2011; Hazen and Downs 2001) of crystalline compounds points out that the maximal thermal expansion should be along the weakest bonding direction.

Two types of solid constructions can be distinguished in the crystal structures of derriksite and demesmaekerite. Those are uranyl selenite chains and interstitial layers built by Cu- and Pb-centered polyhedra. Thus, one could expect the directions of these units' arrangement to be the least prone to expansion. This is actually observed in the structure of **DER**. The lowest expansion occurs

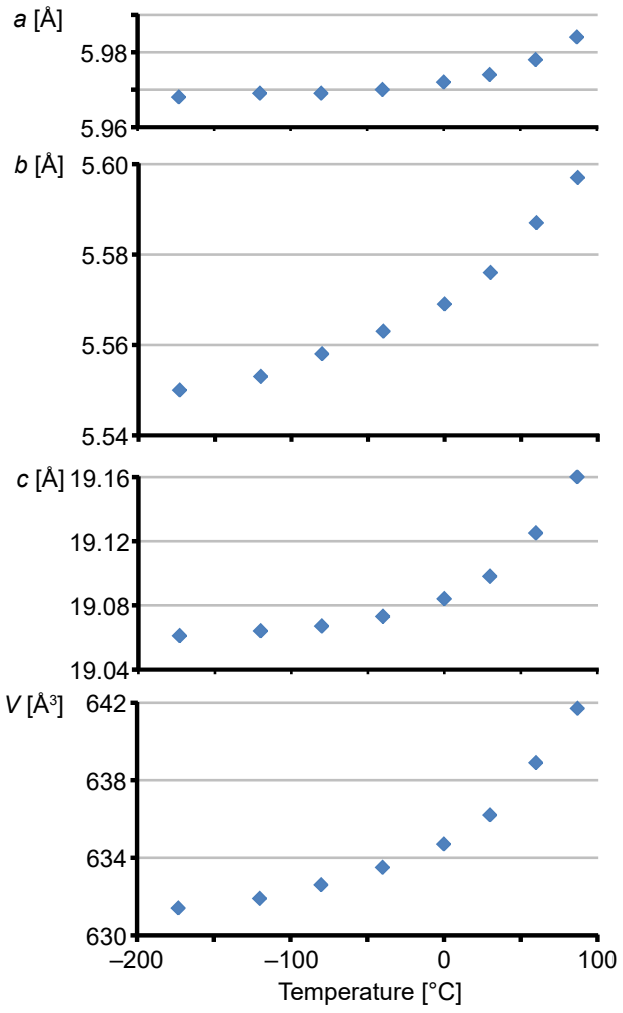

Fig. 5 Unit-cell parameters of **DER** as a function of temperature (–173 to +87 °C) in liquid nitrogen flow (an estimated standard deviations, ESDs, of the unit-cell parameters are within the limits of the symbols).

along the [100], which coincides with the uranyl selenite chain elongation. Uranyl tetragonal bipyramids, selenite groups, and Cu octahedra undergo relatively the same expansion, which can be seen from Tab. 2. Hence, the Cu-bearing layer contributes equally to the rigidity along the [100] and [010]. Linkage of uranyl selenite chains with the Cu-bearing layers *via* covalent and H-bonding systems provides additional rigidity along the [001]. Strong covalent bonding along the [010] occurs only within the octahedral layer, while there is no connection between the U-bearing chains, which causes the largest expansion in this direction. It should also be mentioned that some of the *cis* Cu–O–Cu angular parameters decrease with temperature, which can be attributed to the response of the dense structure of trioctahedral layer to the increase of Cu–O bond lengths.

The thermal expansion dynamics in the structure of **DEM** is more challenging to trace. The first thing that should be worth noting is the change in the orientation of the figure of the TEC with heating. For instance, at low temperatures α_{33} coefficient, which corresponds to the contraction of the structure, almost coincides with the [001], and then it shifts towards the solid diagonal of the unit cell. Although this direction corresponds to the space between the uranyl selenite chains with the deficiency of strong bonds, the contraction of the structure and rotation of the figure of the TEC should be mainly attributed to the orthogonalization of the oblique triclinic angles of the unit cell. This effect was described by Filatov (2008) and recently observed in (Izatulina et al. 2018, 2019). Along the [010], the linkage between the U-bearing chains and interlayer Cu–Pb complex occurs *via* sharing O atoms of the selenite groups, which explains the insignificant expansion of the structure in this direction. Thermal expansion of U, Se, Cu and Pb coordination polyhedra is equivalent, which can be seen from the dynamics of bond lengths and angles with heating (Tab. 3). The maximal expansion of **DER** is observed approximately along the [100], which matches the direction of the thin chain of Cu-centered octahedra and gaps between Cu chains occupied by the Pb cations.

Tab. 4 The main coefficients of the thermal expansion/contraction α_{ii} (i = 1–3) × 10^6 °C^{-1} and orientation of the main axes in the structures of **DER** and **DEM**

Sample	T (°C)	α_{11}	α_{22}	α_{33}	$<\alpha_{11}a$	$<\alpha_{22}b$	$<\alpha_{33}c$
DER	–100	2.5	17.6	4.4	0	0	0
	–50	8.2	29.3	15.7	0	0	0
	0	13.9	40.9	27.0	0	0	0
	50	19.5	52.4	38.2	0	0	0
DEM	–100	36.6	12.3	–3.9	25.2	24.8	5.9
	–50	32.6	14.5	–3.9	32.3	30.7	9.2
	0	29.8	16.3	–4.7	42.4	39.6	15.1
	50	28.5	17.6	–6.5	55.1	51.8	22.4

4. Conclusions

As the result for derriksite, $Cu_4[(UO_2)(SeO_3)_2](OH)_6$, and demesmaekerite, $Pb_2Cu_5[(UO_2)_2(SeO_3)_6(OH)_6](H_2O)_2$, crystal structures refinement in the temperature range of –173 to +87 °C, thermal behavior of their structures was analyzed. In general, the lowest expansion is observed along the direction of uranyl selenite chains, while the largest expansion occurs in the direction normal or inclined to chains, with the low covalent bond distribution density. The crystal structure of demesmaekerite undergoes a contraction of the

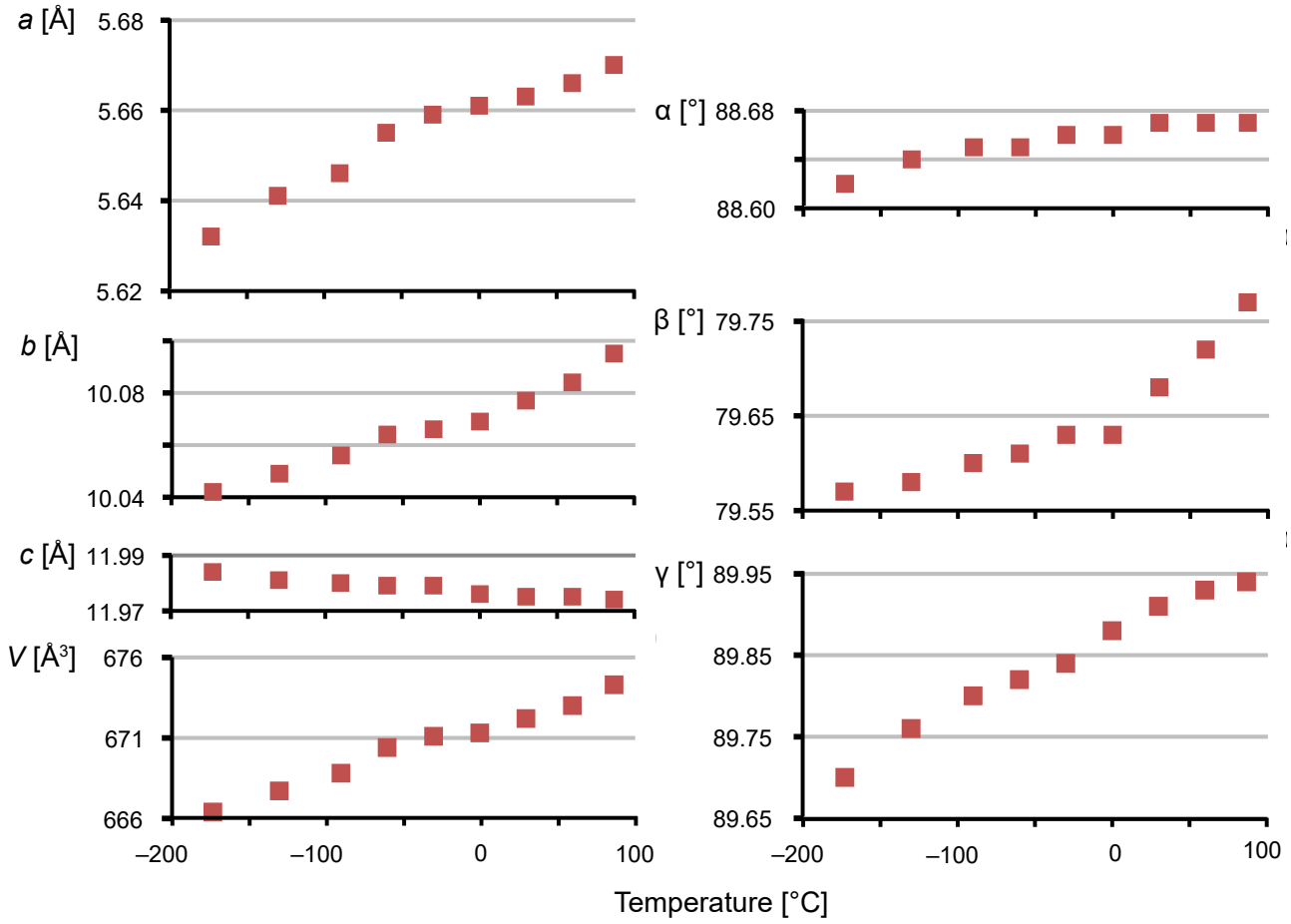

Fig. 6 Unit-cell parameters of DEM as a function of temperature (–173 to +87 °C) in liquid nitrogen flow (ESDs of the unit cell parameters are within the limits of the symbols).

structure during heating, which can be attributed to the orthogonalization of the oblique angles of the triclinic unit cell.

The results of current study allow to expand the common crystal chemical borders of the U^{6+}-bearing minerals and to estimate rather rarely studied parameters such as the strength characteristics of crystal structures. By the current study, it has been documented that uranyl complexes are one of the most stable and rigid blocks in the structural architecture of natural and synthetic uranyl compounds, and they govern the thermal behavior of the whole structure, which is in agreement with the results of recent studies (Gurzhiy et al. 2018, 2020; Kornyakov et al. 2019). These conclusions are valid, regardless of:

1) the dimensionality of U^{6+}-bearing substructural units,
2) both the arrangement and the chemical composition of an interlayer structure.

These observations reasonably justifies an assignment of U^{6+}-bearing units as the fundamental building blocks (FBB) of the entire crystal structures of U^{6+}-compounds and justifies the structural hierarchies based on these FBB (Burns 1999, 2005; Lussier et al. 2016).

Acknowledgments. This research was funded by the Russian Science Foundation (grant 18-17-00018). The XRD and EDX measurements have been performed at the X-ray Diffraction Centre and "Geomodel" Research Centre of the St. Petersburg State University. We are grateful to two anonymous reviewers for useful comments.

Electronic supplementary material. Supplementary crystallographic data are available online at the Journal web site (*http://dx.doi.org/10.3190/jgeosci.315*).

References

Burns PC (1999) The crystal chemistry of uranium. In: Uranium: Mineralogy, Geochemistry and the Environment. Rev Mineral 38: 23–90

Burns PC (2005) U^{6+} minerals and inorganic compounds: insights into an expanded structural hierarchy of crystal structures. Canad Mineral 43: 1839–1894

Cesbron F, Bachet B, Oosterbosch R (1965) La demesmaekerite, sélénite hydraté d'uranium, cuivre et plomb. Bull Soc franc Minéral Cristallogr 88: 422–425

Cesbron F, Oosterbosch R, Pierrot R (1969) Une nouvelle espèce minérale: la marthozite. Uranyl-sélénite de cuivre hydraté. Bull Soc franc Minéral Cristallogr 92: 278–283

Cesbron F, Pierrot R, Verbeek T (1971) La derriksite, $Cu_4(UO_2)(SeO_3)_2(OH)_6 \cdot H_2O$, une nouvelle espèce minérale. Bull Soc franc Minéral Cristallogr 94: 534–537

Chukanov NV, Pushcharovsky DYu, Pasero M, Merlino S, Barinova AV, Möckel S, Pekov IV, Zadov AE, Dubinchuk VT (2004) Larisaite, $Na(H_3O)(UO_2)_3(SeO_3)_2O_2 \cdot 4H_2O$, a new uranyl selenite mineral from Repete mine, San Juan County, Utah, U.S.A. Eur J Mineral 16: 367–374

Clark RC, Reid JS (1995) The analytical calculation of absorption in multifaceted crystals. Acta Crystallogr A51: 887–897

CrysAlisPro Software System (2018) version 1.171.39.44; Rigaku Oxford Diffraction: Oxford, UK

Deliens M, Piret P (1991) La haynesite, sélénite hydraté d'uranyle, nouvelle espèce minérale de la Mine Repete, Comté de San Juan, Utah. Canad Mineral 29: 561–564

Demartin F, Diella V, Donzelli S, Gramaccioli CM, Pilati T (1991) The importance of accurate crystal structure determination of uranium minerals. I. Phosphuranylite $KCa(H_3O)_3(UO_2)_7(PO_4)_4O_4 \cdot 8H_2O$. Acta Crystallogr B47: 439–446

Dolomanov OV, Bourhis LJ, Gildea RJ, Howard JAK, Puschmann H (2009) OLEX2: A complete structure solution, refinement and analysis program. J appl Crystallogr 42: 339–341

Filatov SK (1990) Visokotemperaturnaia Kristallohimia (High-Temperature Crystal Chemistry, in Russian). Nedra, Leningrad, Russia, pp 1–288

Filatov SK (2008) Negative linear thermal expansion of oblique-angle (monoclinic and triclinic) crystals as a common case. Phys Stat Sol B245: 2490–2496

Filatov SK (2011) General concept of increasing crystal symmetry with an increase in temperature. Crystallogr Rep 56: 953–961

Frost RL, Weier ML, Reddy BJ, Čejka J (2006) A Raman spectroscopic study of the uranyl selenite mineral haynesite. J Raman Spectros 37: 816–821

Frost RL, Čejka J, Keeffe EC, Dickfos MJ (2008a) Raman spectroscopic study of the uranyl selenite mineral marthozite $Cu[(UO_2)_3(SeO_3)_2O_2] \cdot 8H_2O$. J Raman Spec, 39: 1413–1418

Frost RL, Reddy BJ, Dickfos MJ (2008b) An application of near infrared and mid-infrared spectroscopy to the study of uranyl selenite minerals: derriksite, demesmaekerite, guilleminite and haynesite. J Near Infrared Spectrosc 16: 455–469

Frost RL, Čejka J, Dickfos MJ (2009a) Raman spectroscopic study of the mineral guilleminite $Ba(UO_2)_3(SeO_3)_2(OH)_4 \cdot 3H_2O$. J Raman Spectrosc 40: 355–359

Frost RL, Čejka J, Dickfos MJ (2009b) Raman spectroscopic study of the uranyl selenite mineral demesmaekerite $Pb_2Cu_5(UO_2)_2(SeO_3)_6(OH)_6 \cdot 2H_2O$. J Raman Spectrosc 40: 476–480

Frost RL, Čejka J, Scholz R, Lopez A, Theiss FL, Xi Y (2014) Vibrational spectroscopic study of the uranyl selenite mineral derriksite $Cu_4[(UO_2)(SeO_3)_2](OH)_6 \cdot H_2O$. Spectrochim Acta A 117: 473–477

Ginderow D, Cesbron F (1983a) Structure de la demesmaekerite, $Pb_2Cu_5(SeO_3)_6(UO_2)_2(OH)_6 \cdot 2H_2O$. Acta Crystallogr C39: 824–827

Ginderow D, Cesbron F (1983b) Structure da la derriksite, $Cu_4(UO_2)(SeO_3)_2(OH)_6$. Acta Crystallogr C39: 1605–1607

Gurzhiy VV, Krivovichev SV, Tananaev IG (2017) Dehydration-driven evolution of topological complexity in ethylamonium uranyl selenates. J Solid State Chem 247: 105–112

Gurzhiy VV, Krzhizhanovskaya MG, Izatulina AR, Sigmon GE, Krivovichev SV, Burns PC (2018) Structure refinement and thermal stability studies of the uranyl carbonate mineral andersonite, $Na_2Ca[(UO_2)(CO_3)_3] \cdot (5+x)H_2O$. Minerals 8: 586

Gurzhiy VV, Kuporev IV, Kovrugin VM, Murashko MN, Kasatkin AV, Plášil J (2019a) Crystal chemistry and structural complexity of natural and synthetic uranyl selenites. Crystals 9: 639

Gurzhiy VV, Tyumentseva OS, Izatulina AR, Krivovichev SV, Tananaev IG (2019b) Chemically induced polytypic phase transitions in the $Mg[(UO_2)(TO_4)_2(H_2O)](H_2O)_4$ (T = S, Se) system. Inorg Chem 58: 14760–14768

Gurzhiy VV, Kornyakov IV, Szymanowski JES, Felton D, Tyumentseva OS, Krzhizhanovskaya MG, Krivovichev SV, Burns PC (2020) Chemically-induced structural variations of a family of $Cs_2[(AnO_2)_2(TO_4)_3]$ (An = U, Np; T = S, Se, Cr, Mo) compounds: thermal behavior, calorimetry studies and spectroscopy characterization of Cs uranyl sulfate and selenate. J Solid State Chem 282: 121077

Hathaway BJ (1984) A new look at the stereochemistry and electronic properties of complexes of the copper(II) ion. In: Complex Chemistry. Structure and Bonding, Volume 57. Springer, Berlin, Heidelberg, 55–118

Hawthorne FC, Ferguson RB (1975) Refinement of the crystal structure of kroehnkite. Acta Crystallogr B31: 1753–1755

Hazen RM, Downs RT (2001) Reviews in Mineralogy and Geochemistry, Volume 41: High-Temperature and High-Pressure Crystal Chemistry. Mineralogical Society of America, Washington, DC, USA. pp 1–596

Izatulina AR, Gurzhiy VV, Krzhizhanovskaya MG, Kuz'mina MA, Leoni M, Frank-Kamenetskaya OV (2018) Hydrated Calcium Oxalates: Crystal Structures, Thermal Stability and Phase Evolution. Cryst Growth Des 18: 5465–5478

Izatulina AR, Gurzhiy VV, Krzhizhanovskaya MG, Chukanov NV, Panikorovskii TL (2019) Thermal behavior and phase transition of uric acid and its dihydrate form, the common biominerals uricite and tinnunculite. Minerals 9: 373

Kampf AR, Sejkora J, Witzke T, Plášil J, Čejka J, Nash BP, Marty J (2017) Rietveldite, $Fe(UO_2)(SO_4)_2(H_2O)_5$, a new uranyl sulfate mineral from Giveaway-Simplot mine (Utah, USA), Willi Agatz mine (Saxony, Germany) and Jáchymov (Czech Republic). J Geosci 62: 107–120

Kornyakov IV, Gurzhiy VV, Szymanowski JES, Zhang L, Perry SN, Krivovichev SV, Burns PC (2019) A novel family of Np(VI) oxysalts: crystal structures, calorimetry, thermal behavior, and comparison with U(VI) compounds. Cryst Growth Des 19: 2811–2819

Krivovichev SV (2008) Structural Crystallography of Inorganic Oxysalts. Oxford University Press, Oxford, UK, pp 1–303

Langreiter T, Kahlenberg V (2015) TEV – a program for the determination and visualization of the thermal expansion tensor from diffraction data. Crystals 5: 143–153

Lussier AJ, Lopez RAK, Burns PC (2016) A revised and expanded structure hierarchy of natural and synthetic hexavalent uranium compounds. Canad Mineral, 54: 177–283

Pierrot R, Toussaint J, Verbeek T (1965) La guilleminite, une nouvelle espèce minérale. Bull Soc franc Minéral Cristallogr 88: 132–135

Sheldrick GM (2015a) SHELXT – Integrated space-group and crystal structure determination. Acta Crystallogr A71: 3–8

Sheldrick GM (2015b) Crystal structure refinement with SHELXL. Acta Crystallogr C71, 3–8

Vochten R, Blaton N, Peeters O, Deliens M (1996) Piretite, $Ca(UO_2)_3(SeO_3)_2(OH)_4 \cdot 4H_2O$, a new calcium uranyl selenite from Shinkolobwe, Shaba, Zaire. Canad Mineral 34: 1317–132